

FULL ARTICLE

Noninvasive detection of nanoscale structural changes in cornea associated with cross-linking treatment

Yi Zhou  | Sergey Alexandrov | Andrew Nolan | Nandan Das | Rajib Dey | Martin Leahy 

Tissue Optics and Microcirculation Imaging Facility, National Biophotonics and Imaging Platform, School of Physics, National University of Ireland, Galway, Ireland

Correspondence

Tissue Optics and Microcirculation Imaging Facility, National Biophotonics and Imaging Platform, National University of Ireland, Galway, Ireland.
Email: martin.leahy@nuigalway.ie

Funding information

STARSTEM, IMCUSTOMEYE, Grant/Award Numbers: 761214, 779960; Irish Research Council, Grant/Award Number: GOIPD/2017/837

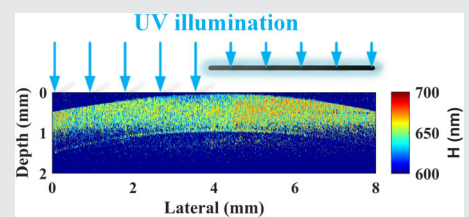
Abstract

Corneal cross-linking (CXL) using ultraviolet-A (UVA) irradiation with a riboflavin photosensitizer has grown from an interesting concept to a practical clinical treatment for corneal ectatic diseases globally,

such as keratoconus. To characterize the corneal structural changes, existing methods such as X-ray microscopy, transmission electron microscopy, histology and optical coherence tomography (OCT) have been used. However, these methods have various drawbacks such as invasive detection, the impossibility for in vivo measurement, or limited resolution and sensitivity to structural alterations. Here, we report the application of oversampling nanosensitive OCT for probing the corneal structural alterations. The results indicate that the spatial period increases slightly after 30 minutes riboflavin instillation but decreases significantly after 30 minutes UVA irradiation following the Dresden protocol. The proposed noninvasive method can be implemented using existing OCT systems, without any additional components, for detecting nanoscale changes with the potential to assist diagnostic assessment during CXL treatment, and possibly to be a real-time monitoring tool in clinics.

KEYWORDS

corneal cross-linking, nanoscale alteration, nanoscale sensitivity, optical coherence tomography, spatial period



1 | INTRODUCTION

Corneal ectasia can severely impair vision, especially in the progressive form caused by the inherent structural

weakness of the cornea [1, 2]. Keratoconus, the most common form of corneal ectasia affecting nearly 1 in 375 individuals globally, is an ocular disorder characterized by corneal degeneration due to corneal thinning that

results in a focally decreased radius of corneal curvature and abnormal wave front aberrations [3–5]. Keratoconus is a noninflammatory, progressive disease resulting in corneal instability in the structure. Sometimes it ultimately may require a corneal transplant. In recent years, a nonsurgical keratoconus treatment, corneal cross-linking (CXL), was proved to be an effective way of halting the progression of keratoconus, meaning patients can avoid a corneal transplant [6–9]. CXL, using a combination of ultraviolet-A (UVA) light with 365 nm central wavelength and a photosensitizer (riboflavin, vitamin B2) for the procedure, shows a physiologic principle of tissue biomechanical modification [10–12]. CXL, which presents to be a minimally invasive treatment to stiffen the corneal stroma by strengthening the connections between collagen fibrils, was first approved by the US Food and Drug Administration in April 2016 [13].

Despite being in clinical use for several years, some of the principles and underlying processes, such as the role of oxygen, the optimal treatment time and the way to monitor and assess the treatment, are still being worked out [14, 15]. The basic theory behind this approach is photopolymerization, which leads to the creation of chemical bonds between collagen and proteoglycans and other proteins within the corneal stroma. Various research studies have been reported that the increase of tissue stiffness is dependent on the modifications of mechanical properties, which have a strong relationship with the ultrastructural alterations within the cross-linked cornea, such as the changes of the characteristics of collagen fibrils [16, 17]. Detection of structural changes in corneal stroma during the cross-linking procedure would allow a more detailed investigation of healing processes or the efficacy of drugs. Characterizing the structural changes could allow in the future to improve optical monitoring and treatment methods to repair damages in the cornea [18–22]. Transmission electron microscopy (TEM) and scanning electron microscopy (SEM) were used to study the relationship between mechanical behavior and changes in the corneal ultrastructure after cross-linking in rabbit eyes [23, 24]. Although the nanoscale structure can be clearly imaged, these technologies will only suit the samples *in vitro*. Another option for detecting ultrastructure in the cornea is histology, which requires the anatomy of the tissue and therefore only applicable for *ex vivo* tissue. Some other methodologies including X-ray microscopy [25] and confocal microscopy [26, 27] also have various limitations, such as harmfulness from radiation damage, small imaging area or shallow imaging depth, causing difficulties in clinical eye diagnostics.

Optical coherence tomography (OCT), first introduced by its name in 1991 for the visualization of

alterations in the human eye by a team in Massachusetts Institute of Technology (MIT), originates from optical low-coherence interferometry and generates two-dimensional or three-dimensional (3D) cross-sectional tomographic images by detecting the echo time delay and intensity of light which is reflected or backscattered from internal structures in tissue [28–30]. OCT has proved to be of significant value in the visualization of transparent, weakly scattering media, such as the cornea, and obtained a substantial impact in the ophthalmology community [15, 31–33]. Efforts made in the last years in OCT technology have also made it possible to image highly scattering tissues, such as in dermatology, gastroenterology, oncology, and interventional cardiology. Given its high-resolution, noninvasive, fast-speed and 3D method, OCT fills the gap between the optical microscopy and currently available clinical imaging methods considering both imaging resolution and depth.

The interest in OCT for ophthalmic applications has rapidly increased in the past years. Refractive surgery on the cornea benefits very much from the existing OCT technology and is also used for phakic intraocular lens implantation. Laser-assisted *in situ* keratomileusis enhancement and lamellar keratoplasty are other applications using OCT technology. In all cases, OCT opened promising therapeutic and diagnostic options in both research and clinical applications in ophthalmology. The spatial and axial resolution of OCT is, however, also limited by the wavelength of the used light source and the used optical components. However, for specific treatments of the eye's cornea, the monitoring of the cross-linking process requires image resolution in the nanometer range as documented using TEM and SEM [23, 34].

In this study, we have presented the application of oversampling nanosensitive OCT (nsOCT), which is proposed to retain the high spatial frequency information in the interference spectra, to probe the structural alterations inside *ex vivo* bovine cornea during CXL treatment with nanoscale sensitivity. The capability of the proposed nsOCT method to detect nanoscale difference has been proved experimentally by distinguishing two periodic Bragg grating samples with known dimensional sizes. The investigation of CXL was performed using the Dresden protocol, which is the gold standard for the CXL treatment. The data of corneas were recorded and analyzed in three-time nodes: (a) the epithelium removal, (b) a 30 minutes riboflavin instillation and (c) a 30 minutes UVA irradiation. We present the oversampling nsOCT B-scans and *en face* results at different corneal depths, showing a consistent consequence. The spatial periods of cornea decreased significantly after 30 minutes riboflavin instillation and

30 minutes UVA irradiation. The results suggest that the oversampling nsOCT can be used to detect nanosized structural changes valuable for corneal treatment methods.

2 | METHODS

2.1 | Principle and demonstration of the oversampling nsOCT

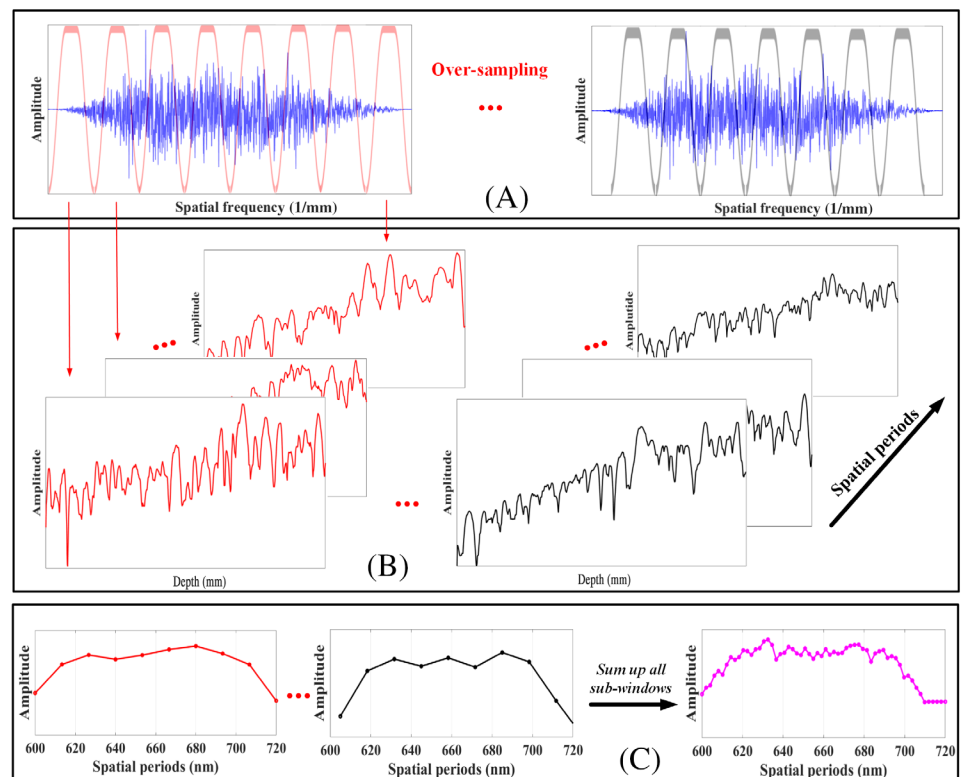
Scattering potential of a 3D object can be reconstructed from the distribution of the complex amplitude of the light scattered by the objective in far zone via 3D inverse Fourier transform [35]. Based on the theory of spectral encoding of spatial frequency approach [36–39], which was demonstrated for quantitative characterization of the structure with nanoscale sensitivity, nsOCT has been proposed to be a label-free depth-resolved sensing technique to probe structural changes at the nanoscale [40–42]. Later nsOCT has been used for the study of the nanometer-scale structural changes of the human tympanic membrane in otitis media [43]. Recently a version of the nsOCT based on the correlation between axial spatial frequency profiles has been published [44]. In this study, oversampling is used to increase the number of points in the reconstructed axial spatial frequency/period profiles. In conventional OCT, high-frequency information has been killed during the inverse Fourier transform, and the axial

resolution is limited in micron level depending on the spectral bandwidth of the light source.

The nsOCT method carries the spectrally encoded axial spatial period from the k -space to the reconstructed object space by encoding each axial spatial frequency with one particular wavelength. The signal processing for nsOCT is illustrated in a flowchart in Figure 1. To realize oversampling nsOCT, we first obtain the processed interference spectra after basically preliminary modifications, including k -space linearization, background noise removal, apodization, and dispersion compensation. Then the processed spectra are decomposed into several sub-bands using Tukey windows as for nsOCT imaging. To minimize the spatial frequency range for one sub-band, we then oversample the spatial frequencies by shifting the window with the same width, that is, the starting point for each processing shifts along with spatial frequency, as illustrated in Figure 1A. The FFT of each sub-band signal has been performed to get the amplitude along all the imaging depths for one spatial frequency range, as shown in Figure 1B. By combining all the oversampling spatial profiles, it is possible to reconstruct the dominant structural size of each voxel by counting the medium spatial periods with the maximum energy contribution, as indicated in Figure 1C.

The collected complex amplitudes of the spectrum are converted to complex amplitudes of spatial frequencies (Vz) based on the following relation:

FIGURE 1 Flowchart for the oversampling nanosensitive optical coherence tomography (nsOCT) signal processing. A, Decompose axial spatial frequencies into multiple sub-bands and shift the dividing windows for oversampling the spatial frequencies. B, FFT of each sub-band and acquire the amplitude along different depths in each particular spatial frequency range. C, Reconstruct and sum up all the spatial period profiles by taking the energy contribution of each sub-band and then obtain the dominant structural size for each voxel



$$V_z = \frac{2n}{\lambda} \quad (1)$$

where n is the refractive index, and λ is the wavelength. The spatial periods (H_z) of the structure can be expressed as follows:

$$H_z = \frac{1}{V_z} = \frac{\lambda}{2n} \quad (2)$$

The nsOCT image can be then constructed by mapping the corresponding dominant spatial period to each voxel with an optimized threshold.

For further experimental validation of the proposed nsOCT method, we used two reflection Bragg gratings with periodicities of 431.6 and 441.7 nm (Corp. Opti-Grate, Florida) as the samples. Each periodic layer was fabricated with sinusoidal refractive index varies 1.483 ± 0.001 . No variation in periodicity vs time if the temperature of usage is $<400^\circ\text{C}$ (the period will be stable better than 1 pm). With the purpose of mimicking an imaging condition similar to real tissue, a two-layer plastic tape was placed on the top of the Bragg gratings and a tissue paper was placed on the bottom, as shown in Figure 2A.

Figure 2A,B shows the conventional intensity-based OCT B-scan and *en face* images, where the structural difference between the Bragg gratings cannot be recognized since the high-frequency information is not available using general OCT processing. While following the proposed nsOCT method, both the nsOCT B-scan and *en face* images were constructed with spatial periods mapping as presented in Figure 2C,D, easily visualizing the nanometer structural difference (~ 10 nm) between two Bragg gratings. The spatial periods of the tape and tissue paper are quite diffused with various values as the structural sizes of them are randomly distributed. From the proof-of-concept demonstrations, we successfully verify that the nsOCT method is a promising way to sense nanoscale structural alterations along the depth axis.

Further, to clarify the difference between oversampling nsOCT and the previous nsOCT method, we have added both simulation and experiment results. In the simulation, we produce seven samples with different axial periodicities of 425, 428, 431, 434, 437, 440, and 443 nm. As shown in Figure 3, the structural difference of 3 nm can be distinguished by the oversampling nsOCT. However, nsOCT without oversampling can only detect the difference of 6 nm but cannot distinguish the 3 nm difference. In the

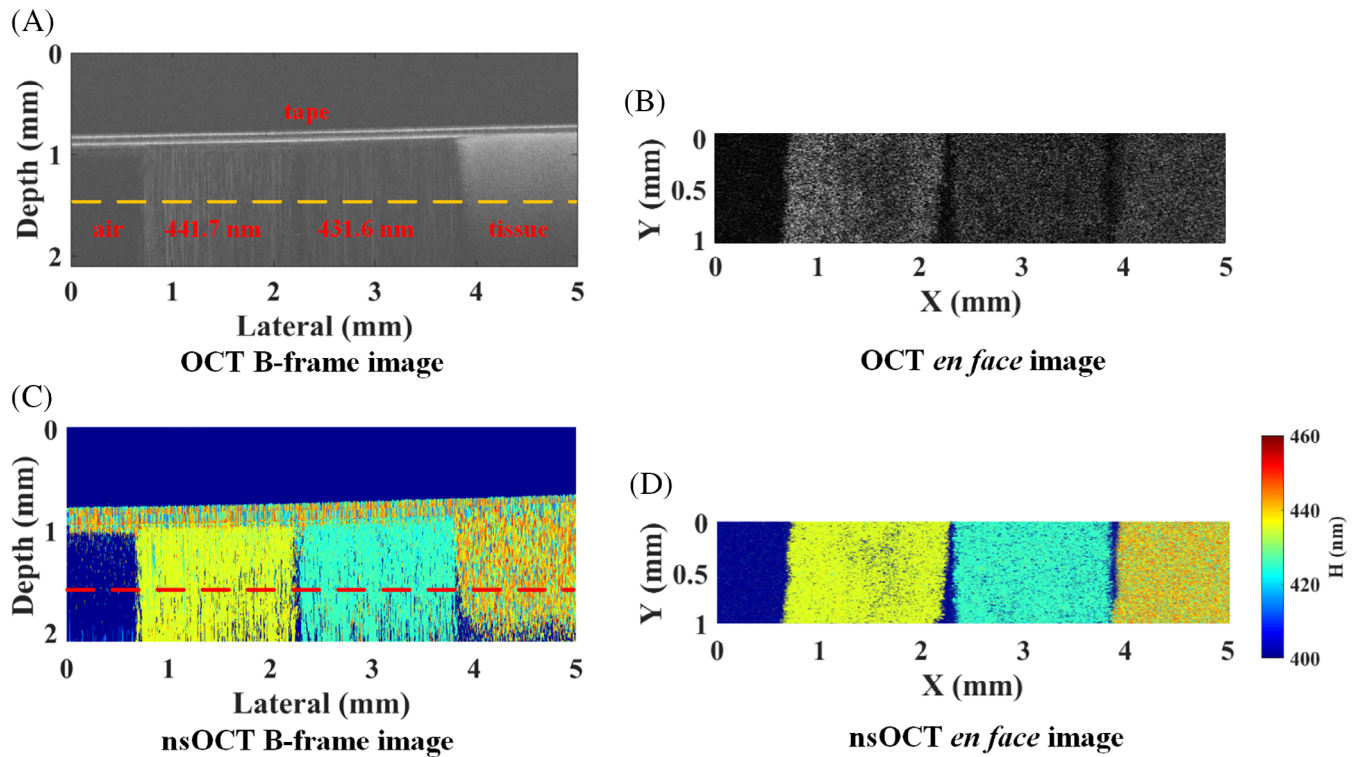


FIGURE 2 Experimental validation of the oversampling nanosensitive optical coherence tomography (nsOCT) method by both B-scan and *en face* images. The two periodicity-different Bragg gratings and a tissue paper were covered under a two-layer tape. A,B, Conventional intensity-based OCT B-scan and *en face* image at the depth marked by the dashed line. C,D, The corresponding nsOCT B-scan and *en face* image with spatial periods mapping, visualizing the nanoscale structural differences between the samples. The color bar presents the spatial periods with unit nanometer

experiment, we still use the Bragg gratings for the demonstration. For the Bragg grating with 431.6 nm periodicity, we measure 430.4 nm (error: 1.2 nm) by oversampling nsOCT while 428.2 nm (error: 3.4 nm) by the previous nsOCT method, as shown in Figure 4. It also demonstrates that nsOCT after oversampling can provide a higher measurement accuracy. Another result of the Bragg grating with 441.7 nm periodicity is attached in the supplementary files Figure S1, also showing an improved sensitivity after the oversampling process.

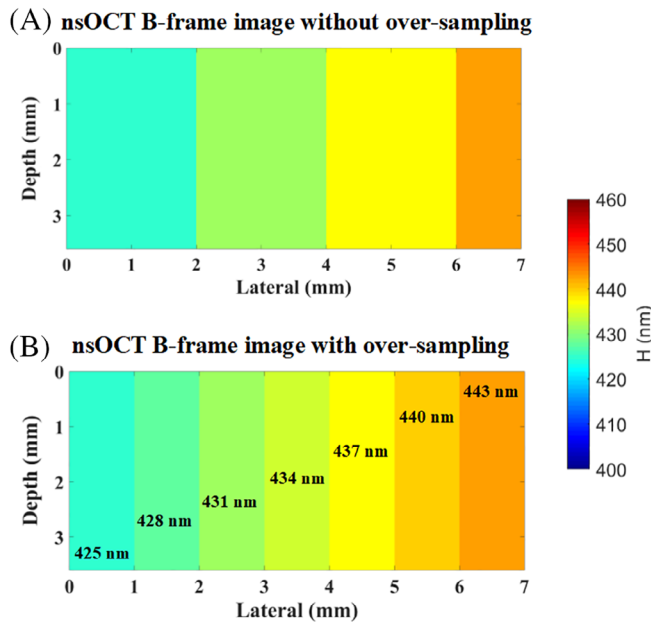


FIGURE 3 Simulation results of nanosensitive optical coherence tomography (nsOCT) without and with oversampling. A, nsOCT without oversampling can detect the difference of 6 nm but cannot distinguish 3 nm difference; B, nsOCT with oversampling is able to distinguish the structural difference of 3 nm

2.2 | Ex vivo bovine CXL experiment

In the CXL experiments, we chose bovine corneas for a more consistent sample quality from the local abattoir. The bovine eyes were harvested in the evening of slaughter from a local abattoir (Athenry Quality Meats Ltd., County Galway, Ireland) within 2 hours postmortem and stored at 4°C. The abattoir granted permission for the eyes to be used in research. Eye globes with intact epithelium and clear cornea were selected for the ex vivo studies. We first removed the epithelium with a stainless-steel spatula. The CXL process was performed in a dark environment using riboflavin (MedioCROSS M, 0.1% Riboflavin, 1.1% HPMC) as the photosensitizer and final irradiation with UV-A light (UV-XTM 2000, IROC Innocross, Zurich, Switzerland) with a illumination spot size of 9.5 mm, 3.0 mW/cm² intensity and energy dose of 5.4 J/cm².

Following the Dresden protocol, which is the current gold standard of CXL treatment, we conducted the structural detections at the three treating steps including immediately after epithelial removal, after 30 minutes riboflavin instillation, and after 30 minutes UVA irradiation with a further continuous installation every 2 minutes.

For the data acquisition, a commercial spectral-domain OCT system (Telesto III; Thorlabs, Inc., New Jersey) with an objective lens LSM03 (NA = 0.055, lateral resolution = 13 μm) was used in our experiments. This high-resolution OCT system, operating at the central wavelength of 1300 nm with sensitivity 96 dB @76 kHz rate, can reach an axial resolution of 5.5 μm and imaging depth of 3.6 mm in air.

3 | RESULTS

We used a laser scanning confocal microscopy system (FV 3000, Olympus) to investigate the differences

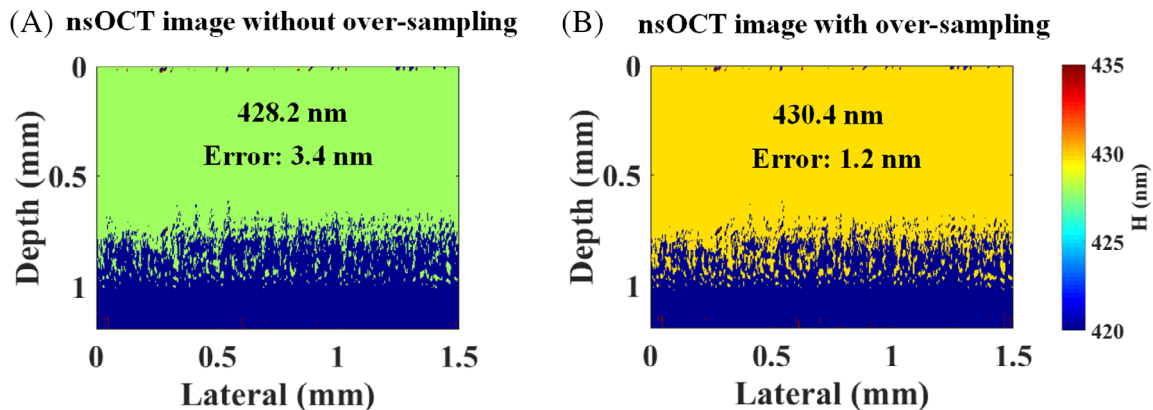


FIGURE 4 Experimental results of the Bragg grating with the axial periodicity of 431.6 nm. A, The nanosensitive optical coherence tomography (nsOCT) without oversampling presents a 428.2 nm structural size. Error is 3.4 nm. B, The nsOCT with oversampling shows a 430.4 nm structural size. Error is 1.2 nm. The color bar presents the spatial periods with unit nanometers

between the untreated and treated corneas. We used a 405 nm excitation wavelength and an objective lens with an NA of 0.85 (UPLSAPO 20XO) for the imaging process. The confocal microscopy images of the virgin and treated corneas are presented in Figure 5. The virgin corneas consisted of highly reflective and well-demarcated cell nuclei with an oval shape, indicated by white arrows. Neither keratocyte processes nor collagen fibers could be visualized. However, the crosslinked cornea was

populated with some reflective interconnected stellate structures. These structures contained elongated nuclei and keratocyte apoptotic bodies. The confocal microscope images show that the CXL has occurred during the CXL treatment.

Figure 6A,C,E shows the intensity-based OCT B-scans for the three processing steps, respectively. We could see that the cornea thickness decreased in both the center and periphery areas after the CXL process, as shown in

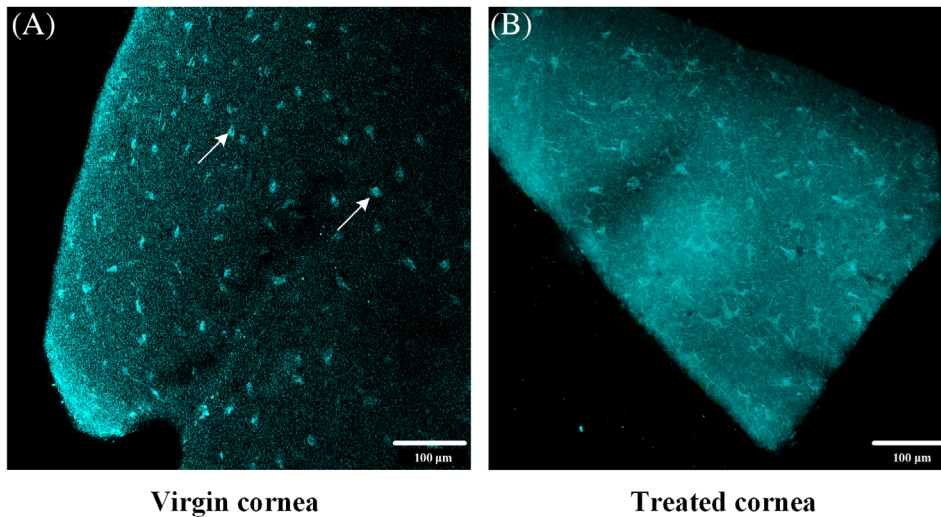


FIGURE 5 Confocal microscopy images of the virgin and treated cornea. A, The virgin corneas consist of highly reflective and well-demarcated cell nuclei with an oval shape, indicated by white arrows. B, The treated cornea is populated with some reflective interconnected stellate structures, containing elongated nuclei and keratocyte apoptotic bodies. The scale bar is 100 μm

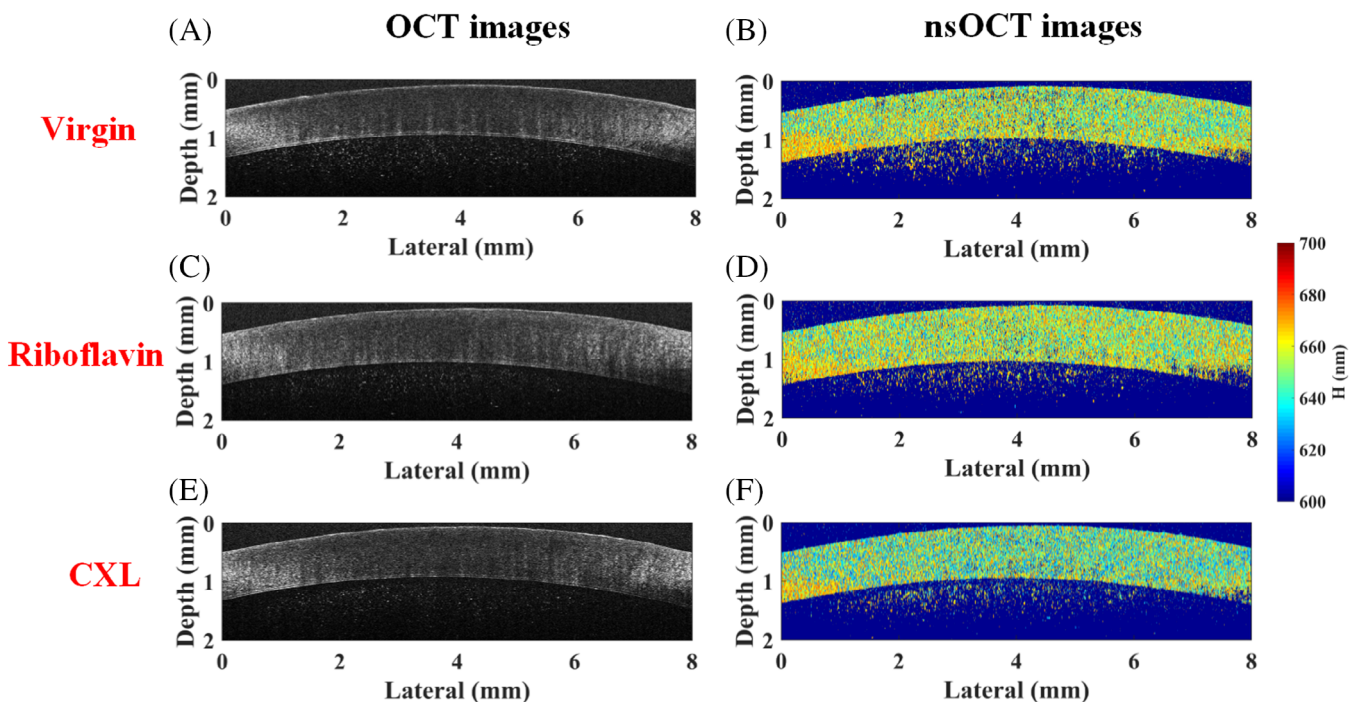


FIGURE 6 B-scans of ex vivo bovine cornea during corneal cross-linking (CXL) treatment at three treating steps. A,B, Both conventional OCT and nanosensitive optical coherence tomography (nsOCT) images acquired immediately after epithelial removal. C,D, Images constructed after 30 minutes riboflavin instillation and E,F, after 30 minutes ultraviolet-A (UVA) irradiation while finishing the treatment. The color bar presents the spatial periods with unit nanometers

the supplementary file Figure S2. However, the conventional OCT images cannot identify any structural changes smaller than the resolution limit and no structural differences inside corneas can be identified. Here, we applied the proposed nsOCT method for analyzing the structural responses during CXL treatment, showing B-scans with spatial periods mapping, as presented in Figure 6B,D,F. The nsOCT B-scans show that there are no observable structural alterations between the virgin cornea and the cornea after 30 minutes riboflavin instillation, only presenting a minor increase after riboflavin immersion due to the higher refractive index of riboflavin. However, the spatial periods had an obvious decrease after 30 minutes UVA irradiation, meaning that the structural size decreased significantly after the CXL treatment. In Figure 6F, the spatial periods after the CXL process were clearly detected to be smaller by several nanometers compared to Figure 6B,D.

To quantitatively demonstrate the structural variations associated with CXL treatment, we also investigated the histograms and boxplots of spatial period distributions for B-scans at all three steps. Figure 7A-C indicates the spatial period results for one of the bovine corneas. The mean spatial periods of the virgin cornea, the cornea after 30 minutes riboflavin instillation and after 30 minutes UVA irradiation were measured to be 657.1, 658.1, and 649.6 nm, respectively, illustrating the slightly larger spatial size after riboflavin immersion but substantially smaller after the CXL procedure. In the meantime, the histograms of spatial period distributions also show that the treated cornea has shifted to be smaller structural sizes.

Further, we have conducted a series of repeating experiments on different bovine eyes under the same CXL protocol and signal processing. Analyzing the experimental data of 10 bovine eyes associated with

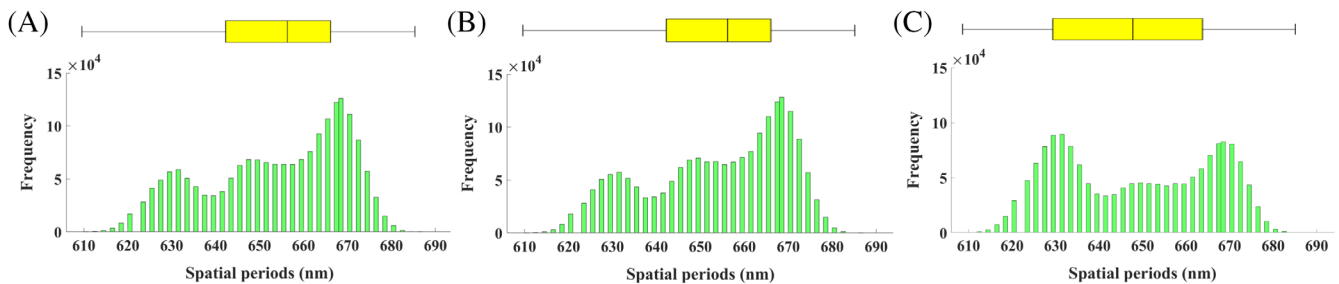


FIGURE 7 Histogram and boxplot of spatial period distributions inside cornea associated with corneal cross-linking (CXL) treatment. A, Virgin cornea with the mean spatial period of 657.1 nm. B, The cornea after 30 minutes riboflavin instillation with the mean value of 658.1 nm. C, The crosslinked cornea with the mean value of 649.6 nm, with the histogram showing a shift towards lower spatial period compared with (A) and (B)

TABLE 1 The intensity changes between the virgin cornea and cross-linked cornea during the CXL treatment

Bovine corneas	Mean intensity values (dB)			
	Virgin	Treated	Shift	%
S1	35.86	35.57	-0.29	-0.81
S2	35.99	35.31	-0.68	-1.89
S3	35.58	34.96	-0.62	-1.74
S4	36.01	36.55	+0.54	+1.50
S5	35.90	35.36	-0.54	-1.50
S6	35.62	36.01	+0.39	+1.09
S7	35.88	36.13	+0.25	+0.70
S8	35.79	35.99	+0.20	+0.56
S9	36.03	35.69	-0.34	-0.94
S10	35.86	35.32	-0.54	-1.50
Mean	35.85 ± 0.15	35.69 ± 0.48	-0.16 ± 0.46	(-0.45 ± 1.23)

Abbreviation: CXL, corneal cross-linking.

Bovine corneas	Mean spatial periods (nm)			
	Virgin	Treated	Shift	%
S1	657.1	649.6	-7.5	-1.14
S2	652.1	638.5	-13.6	-2.09
S3	656.3	649.2	-7.1	-1.08
S4	654.3	648.1	-6.2	-0.95
S5	653.2	649.6	-3.6	-0.55
S6	651.7	646.9	-4.8	-0.74
S7	653.6	648.9	-4.7	-0.72
S8	653.9	647.3	-6.6	-1.01
S9	654.3	649.6	-4.7	-0.72
S10	652.6	647.3	-5.3	-0.81
Mean	653.9 ± 1.7	647.5 ± 3.3	-6.4 ± 2.8	(-0.98 ± 0.43)

TABLE 2 The spatial period changes of the virgin cornea and cross-linked cornea during the CXL treatment

Abbreviation: CXL, corneal cross-linking.

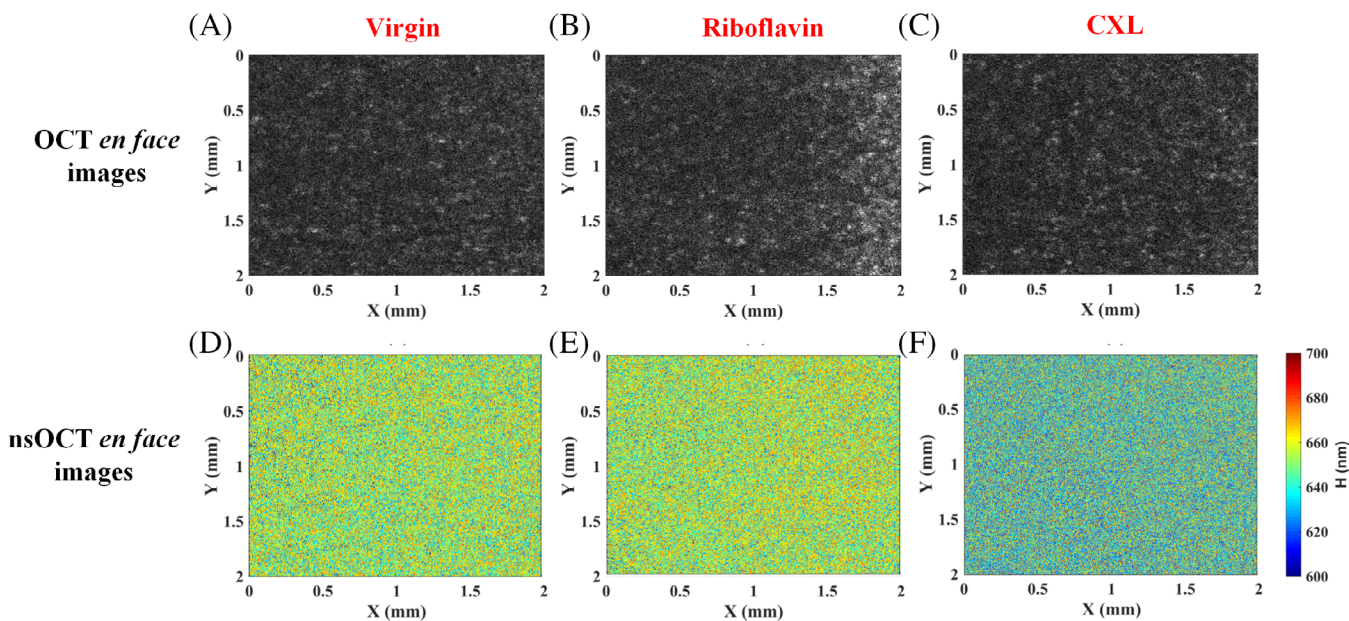


FIGURE 8 Conventional optical coherence tomography (OCT) and nanosensitive OCT (nsOCT) *en face* images at the three key treating steps during corneal cross-linking (CXL) treatment. A-C, Conventional intensity-based OCT *en face* images of the cornea after epithelium removal, after 30 minutes riboflavin instillation and after 30 minutes ultraviolet-A (UVA) illumination, respectively. D-F, The corresponding nsOCT *en face* images with spatial period mapping, presenting the nanoscale structural alterations. The *en face* images were constructed at the depth of $\sim 500 \mu\text{m}$. The color bar presents the spatial periods with unit nanometers

CXL treatment, we made a summary of both the intensity and spatial period shifts as presented in Tables 1 and 2, respectively. We found that the intensity values fluctuated both negatively and positively with no continuous change in one single way, that is, it is not possible to detect the variations during the CXL process by conventional intensity-based OCT. Additionally, we included the intensity histograms of the virgin cornea, the cornea after 30 minutes of riboflavin instillation, and the treated cornea in Figure S3. Again,

we cannot observe any obvious intensity shifts between them.

Summarizing all the experimental sets using the proposed oversampling nsOCT method, we evaluated that the spatial period has changed from $653.9 \pm 1.7 \text{ nm}$ (mean \pm SD) of the virgin corneas to $647.5 \pm 3.3 \text{ nm}$ of the treated corneas. The spatial periods inside the cornea have decreased $-6.4 \pm 2.8 \text{ nm}$ with the percentage of $(-0.98 \pm 0.43)\%$ after CXL treatment. Furthermore, one can also notice that there is a consistent decrease of

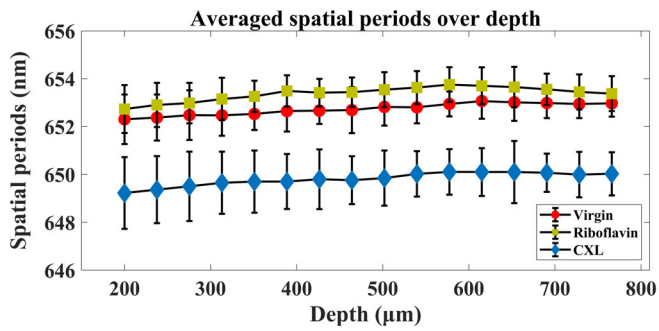


FIGURE 9 Mean spatial periods at various corneal depths for the virgin cornea, the cornea after 30 minutes riboflavin instillation and the cross-linked cornea, indicated by red, yellow and blue color, respectively

spatial period for all the bovine corneas in the experiments, providing a reasonably convincing verification of the nanoscale structural changes associated with the CXL treatment.

The acquisition of 3D volumetric data was used to obtain *en face* images along with different imaging depths. Each *en face* image was obtained over an area with $2 \times 2 \text{ mm}^2$ size and 400×400 A-lines. The treatment was performed with the same protocol as described above. The conventional OCT *en face* images (Figure 8A-C) is not able to resolve any features that could indicate any changes due to the CXL procedure. Nonetheless, the nsOCT *en face* images could visualize the nanoscale alterations especially between the virgin cornea and cross-linked cornea, showing a minor spatial period change after the treatment, as indicated in Figure 8D-F. In the result, the mean spatial periods of *en face* data of the virgin cornea, the cornea after 30 minutes riboflavin instillation and the cross-linked cornea were calculated to be 653.2, 654.3, and 648.6 nm, respectively. To evaluate the change of the nsOCT *en face* images at different depths, a series of scans at increasing depth were assembled in Video S1.

Figure 9 shows the spatial period (Y-axis) along with a depth (X-axis) from 200 to 770 μm computed at depth intervals of 38 μm step width. The change of the spatial period for each treatment step is easily recognizable in Figure 9. The spatial periods for a virgin bovine cornea (red circles) are consistently smaller than those for a cornea treated with riboflavin (yellow squares). A significant change occurs after the 30 minutes of UVA irradiation and the values of the spatial periods reduce by about 3 nm from 652 to 649 nm. Interestingly, we have zoomed in the plot of the spatial periods of the treated cornea and we find a slight increase over the corneal depth, as presented in Figure S4. It is assumed that either the crosslinking

process is affected by adjacent biochemical reactions initiated by the superficial UVA irradiation. The superficial structural changes may generate a dominant spatial periodicity that is propagating into the overall signal range and creating an effect that deeper regions appear to change structural sizes in conjunction with the top layers. However, it is not yet possible to confirm the reasons at this stage, more research studies will be required in the future.

Based on the values plotted in Figure 9, a paired *t* test was performed (samples size 10 per group) which confirmed the high significance ($P < 10^{-4}$) between the virgin corneas and the group after 30 minutes riboflavin instillation. The p-value test for spatial changes between the virgin and CXL treated corneas provided an even larger significance $P < 10^{-13}$.

4 | DISCUSSION

The experimental results of Bragg gratings with known structural sizes have demonstrated the feasibility of the oversampling nsOCT method to distinguish the nanoscale structural alterations in both B-scan and *en face* images. In the study of ex vivo bovine corneas associated with CXL treatment, both the conventional intensity-based OCT images and the corresponding nsOCT images were constructed for the virgin cornea after epithelial removal, the cornea after 30 minutes riboflavin instillation and after 30 minutes UVA irradiation. From the conventional OCT images, we can hardly recognize the internal structural changes of the cornea due to the limited axial resolution of several micrometers. Nonetheless, our investigation using the nsOCT modality could detect the ultrastructural variations inside the cornea during CXL treatment, showing that the spatial periods slightly increased after 30 minutes riboflavin instillation but significantly decreased after 30 minutes UVA irradiation.

According to the existing reports, the structural size inside the cornea should decrease after riboflavin absorption due to the dehydration from the hypertonic photosensitizer solution. In our study, we found an increased spatial period after 30 minutes riboflavin instillation in a dark environment. We think the reason we got opposite results to the TEM or SEM method is because of the increase of refractive index inside cornea after riboflavin immersion. In the OCT system, we detect the optical path difference that depends on both the physical structural size and the refractive index of the sample. The minor increment of the spatial period after 30 minutes riboflavin instillation may be related to the higher refractive index of riboflavin compared to the cornea itself. The mean refractive index inside the stroma will thereby

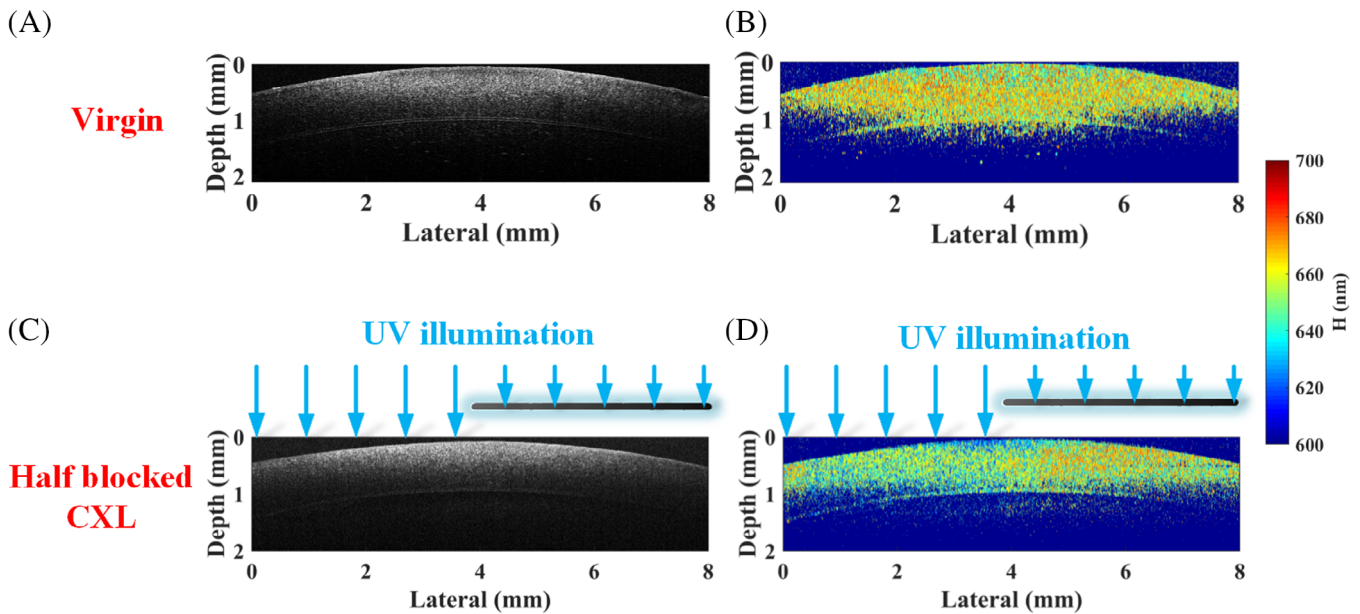


FIGURE 10 A control experiment with the cornea half blocked from ultraviolet-A (UVA) irradiation. A,B, Conventional intensity-based optical coherence tomography (OCT) and nanosensitive OCT (nsOCT) images of the virgin cornea. C, The conventional OCT image of the half cross-linked cornea using a UVA irradiation block on the right half. D, The corresponding nsOCT image of the half cross-linked cornea, illustrating the nanoscale structural difference between the left half and right half in the same B-scan. The color bar presents the spatial periods with unit nanometer

increase when riboflavin penetrates inside the cornea, resulting in a larger spatial period.

To investigate the interfibrillar distance and fibril diameter changes of corneal stroma after CXL treatment, a few methods, such as TEM, SEM, and X-ray imaging, have been discussed in the previous literature. Sibillano et al [25] studied the ex vivo bovine corneas using small-angle X-ray scattering microscopy and revealed that the interfibrillar distance decreased from ~ 62 nm (virgin cornea) to ~ 56 nm (treated cornea). The results also concluded the decrease in the fibril shell thickness from ~ 11 nm to ~ 9 nm after CXL treatment because of the effect of cross-linking within proteoglycan core proteins, resulting in a decreased spatial periods. The similar results on structural changes associated with the CXL process were also reported by Ho, Leona et al [45], Freund et al [46] and Cheng and Pinky [47], showing a good agreement with the proposed nsOCT method. More results have also been reported on the rabbit, porcine and sheep corneas. For instance, Hayes et al [20, 24] found that the fiber diameter of in vitro porcine cornea increased while the interfibrillar spacing decreased. Ex vivo, CXL treatment on sheep corneal tissue samples was associated with slight decreases of collagen intermolecular spacing.

Further, dehydration may be one of the factors contributing to the structural changes during CXL treatment, especially for ex vivo samples. Therefore, to ensure that the structural alterations are induced by CXL treatment

other than some other factors, such as dehydration, a control experiment was arranged. The bovine eye was treated in the same CXL procedure as mentioned before, except that half of the cornea was blocked from the UVA illumination.

The virgin cornea was imaged immediately after removing the epithelium, as Figure 10A shows the intensity-based OCT image and Figure 10B presents the nsOCT image. Then, the riboflavin was dropped on the entire cornea for 30 minutes in a dark environment. In the last step, different from the previous process, a blocking long-pass filter was used to stop the UVA illumination in the right half of the cornea. As presented in Figure 10C, the CXL treatment will only occur in the left half of the cornea, as the UVA light cannot reach the right half. We calculated that the spatial period of the left half was 647.9 nm while the right half is 653.6 nm, also showing a decreased spatial period after CXL treatment. The corresponding nsOCT image, shown in Figure 10D, demonstrated the nanoscale structural differences between left and right half of the same cornea.

5 | CONCLUSION

In this study, we reported that the nanostructural changes inside ex vivo bovine cornea associated with CXL treatment can be clearly detected by the proposed

oversampling nsOCT method. Multiple experiments on several groups of samples have consistently shown that the spatial periods inside corneal stroma decreased slightly after 30 minutes riboflavin instillation and UVA irradiation. *En face* nsOCT images at different corneal depths have also confirmed the consistent consequences, demonstrating the nanoscale structural decrease after the CXL treatment.

To the best of our knowledge, there are no clear tools or procedures to follow up with patient corneal monitoring during CXL treatment. The currently preferred procedure is epithelium mapping which reflects the behavior of the other layers of the cornea, but it is not capable of epi-off surgery or real-time ultrastructural inspection. The proposed method can be implemented using the existing OCT system, without any additional components; therefore, it can be relatively straightforward to be applied in *in vivo* tissues and translated to clinical use as a novel imaging system. Due to its fast, noninvasive detecting method and nanoscale sensitivity, this unique technology has potential to be an indicator in diagnostic assessment associated with CXL treatment, and possibly to be a real-time monitoring tool in clinics as a fast way to receive feedback from patient's tissue. Future work will aim to implement this method for *in vivo* corneal monitoring associated with CXL treatment, including monitoring the nanoscale structural variations at the different treatment steps and also the postoperative assessment.

ACKNOWLEDGMENTS

The authors would like to thank Cerine Lal, Anand Arangath, Ryan McAuley and Kai Neuhaus for their help with the fruitful discussions. This project has received funding from the STARSTEM, IMCUSTOMEYE research and innovation programme under grant agreement nos. 761214 and 779960. The materials presented and views expressed here are the responsibility of the author(s) only. The EU Commission takes no responsibility for any use made of the information set out. N.D. received funding from Irish Research Council (IRC), under Government of Ireland postdoctoral fellowship with project ID: GOIPD/2017/837. The authors also acknowledge the facilities and scientific and technical assistance of the Centre for Microscopy and Imaging at the National University of Ireland Galway.

CONFLICT OF INTEREST

The authors declare no financial or commercial conflict of interest.

ORCID

Yi Zhou  <https://orcid.org/0000-0003-1529-1114>

Martin Leahy  <https://orcid.org/0000-0003-1558-4574>

REFERENCES

- [1] J. A. Gomes, D. Tan, C. J. Rapuano, M. W. Belin, R. Ambrósio Jr., J. L. Guell, F. Malecaze, K. Nishida, V. S. Sangwan, *Cornea* **2015**, *34*, 359.
- [2] S. M. Kymes, J. J. Walline, K. Zadnik, J. Sterling, M. O. Gordon, Collaborative Longitudinal Evaluation of Keratoconus Study Group, *Am. J. Ophthalmol.* **2008**, *145*, 611.
- [3] V. M. Tur, C. MacGregor, R. Jayaswal, D. O'Brart, N. Maycock, *Surv. Ophthalmol.* **2017**, *62*, 770.
- [4] D. A. Godefrooij, G. A. De Wit, C. S. Uiterwaal, S. M. Imhof, R. P. Wisse, *Am. J. Ophthalmol.* **2017**, *175*, 169.
- [5] M. Romero-Jiménez, J. Santodomingo-Rubido, J. S. Wolffsohn, *Contact Lens Anterior Eye* **2010**, *33*, 157.
- [6] J. L. Alio, A. Abbouda, D. D. Valle, J. M. B. del Castillo, J. A. G. Fernandez, *J. Ophthalmic Inflamm. Infect.* **2013**, *3*, 47.
- [7] K. M. Meek, S. Hayes, *Ophthalmic Physiol. Opt.* **2013**, *33*, 78.
- [8] E. Chan, G. R. Snibson, *Clin. Exp. Optom.* **2013**, *96*, 155.
- [9] G. R. Snibson, *Clin. Experiment. Ophthalmol.* **2010**, *38*, 141.
- [10] F. Raiskup, E. Spoerl, *Ocul. Surf.* **2013**, *11*, 65.
- [11] J. B. Randleman, S. S. Khandelwal, F. Hafezi, *Surv. Ophthalmol.* **2015**, *60*, 509.
- [12] E. Spörl, F. Raiskup-Wolf, L. Pillunat, *Klin. Monatsbl. Augenh.* **2008**, *225*, 131.
- [13] B. H. Jeng, M. Farid, S. V. Patel, I. R. Schwab, *Ophthalmology* **2016**, *123*, 2270.
- [14] B. J. Blackburn, S. Gu, M. R. Ford, V. de Stefano, M. W. Jenkins, W. J. Dupps, A. M. Rollins, *Invest. Ophthalmol. Vis. Sci.* **2019**, *60*, 41.
- [15] Y. Zhou, Y. Wang, M. Shen, Z. Jin, Y. Chen, Y. Zhou, J. Qu, D. Zhu, *J. Biomed. Opt.* **2019**, *24*, 105001.
- [16] E. Spoerl, M. Huhle, T. Seiler, *Exp. Eye Res.* **1998**, *66*, 97.
- [17] G. Wollensak, E. Iomdina, *Acta Ophthalmol.* **2009**, *87*, 48.
- [18] S. H. Chang, A. Eliasy, K. J. Chen, Y. R. Ji, T. H. Young, T. J. Wang, C. E. Willoughby, K. J. Hamill, A. Elsheikh, *J. Refract. Surg.* **2018**, *34*, 264.
- [19] S. Choi, S.-C. Lee, H.-J. Lee, Y. Cheong, G.-B. Jung, K.-H. Jin, H.-K. Park, *Lasers Med. Sci.* **2013**, *28*, 1289.
- [20] S. Hayes, C. Boote, C. S. Kamma-Lorger, M. S. Rajan, J. Harris, E. Dooley, N. Hawksworth, J. Hiller, N. J. Terill, F. Hafezi, *PLoS One* **2011**, *6*, e22405.
- [21] E. Spoerl, N. Terai, F. Scholz, F. Raiskup, L. E. Pillunat, *J. Refract. Surg.* **2011**, *27*, 452.
- [22] H. R. Vellara, D. V. Patel, *Clin. Exp. Optom.* **2015**, *98*, 31.
- [23] G. Wollensak, M. Wilsch, E. Spoerl, T. Seiler, *Cornea* **2004**, *23*, 503.
- [24] S. Hayes, C. S. Kamma-Lorger, C. Boote, R. D. Young, A. J. Quantock, A. Rost, Y. Khatib, J. Harris, N. Yagi, N. Terrill, *PLoS One* **2013**, *8*, e52860.
- [25] T. Sibillano, L. De Caro, F. Scattarella, G. Scarcelli, D. Siliqi, D. Altamura, M. Liebi, M. Ladisa, O. Bunk, C. Giannini, *J. Appl. Cryst.* **2016**, *49*, 1231.
- [26] K. M. Bottós, C. V. Regatieri, J. L. Dreyfuss, A. A. Lima-Filho, H. B. Nader, P. Schor, W. Chamon, *J. Refract. Surg.* **2008**, *24*, S715.
- [27] I. B. Damgaard, Y.-C. Liu, A. K. Riau, E. P. W. Teo, M. L. Tey, C. L. Nyein, J. S. Mehta, *Sci. Rep.* **2019**, *9*, 4479.
- [28] D. Huang, E. A. Swanson, C. P. Lin, J. S. Schuman, W. G. Stinson, W. Chang, M. R. Hee, T. Flotte, K. Gregory, C. A. Puliafito, *Science* **1991**, *254*, 1178.
- [29] J. M. Schmitt, *IEEE J. Sel. Top. Quantum Electron.* **1999**, *5*, 1205.

- [30] W. Drexler, U. Morgner, R. K. Ghanta, F. X. Kärtner, J. S. Schuman, J. G. Fujimoto, *Nat. Med.* **2001**, *7*, 502.
- [31] E. Götzinger, M. Pircher, B. Baumann, C. Hirn, C. Vass, C. Hitzenberger, *J. Biophotonics* **2008**, *1*, 129.
- [32] Y. Li, O. Tan, R. Brass, J. L. Weiss, D. Huang, *Ophthalmology* **2012**, *119*, 2425.
- [33] J. G. Fujimoto, *Nat. Biotechnol.* **2003**, *21*, 1361.
- [34] S. P. Veres, J. M. Harrison, J. M. Lee, *J. Orthop. Res.* **2013**, *31*, 1907.
- [35] M. Born, E. Wolf, *Principles of Optics: Electromagnetic Theory of Propagation, Interference and Diffraction of Light*, Elsevier, Oxford, England **2013**.
- [36] S. A. Alexandrov, S. Uttam, R. K. Bista, K. Staton, Y. Liu, *Appl. Phys. Lett.* **2012**, *101*, 033702.
- [37] S. A. Alexandrov, S. Uttam, R. K. Bista, C. Zhao, Y. Liu *Opt. Exp. Dermatol.* **2012**, *20*, 9203.
- [38] S. A. Alexandrov, J. McGrath, H. Subhash, F. Boccafoschi, C. Giannini, M. Leahy, *Sci. Rep.* **2015**, *5*, 13274.
- [39] S. Alexandrov, J. McGrath, C. J. Sheppard, F. Boccafoschi, C. Giannini, T. Sibillano, H. Subhash, J. Hogan, M. Leahy, *J. Biophotonics* **2018**, *11*, e201700385.
- [40] S. A. Alexandrov, H. M. Subhash, A. Zam, M. Leahy, *Nano-scale* **2014**, *6*, 3545.
- [41] S. Alexandrov, H. Subhash, M. Leahy, Z. Azhar, (National University of Ireland Galway), *European Patent EP3055643 B1*, 2014 and *U.S. Patent 10,012,492*, **2018**.
- [42] S. Alexandrov, H. Subhash, M. Leahy, *Quantum Electron.* **2014**, *44*, 657.
- [43] R. Dsouza, J. Won, G. L. Monroy, M. C. Hill, R. G. Porter, M. A. Novak, S. A. Boppart, *Sci. Rep.* **2018**, *8*, 8777.
- [44] S. Alexandrov, P. M. McNamara, N. Das, Y. Zhou, G. Lynch, J. Hogan, M. Leahy, *Appl. Phys. Lett.* **2019**, *115*, 121105.
- [45] L. T. Ho, A. M. Harris, H. Tanioka, N. Yagi, S. Kinoshita, B. Caterson, A. J. Quantock, R. D. Young, K. M. Meek, *Matrix Biol.* **2014**, *38*, 59.
- [46] D. Freund, R. McCally, R. Farrell, S. Cristol, N. L'Hernault, H. Edelhauser, *Invest. Ophthalmol. Vis. Sci.* **1995**, *36*, 1508.
- [47] X. Cheng, P. M. Pinsky, *J. Royal Soc. Interface* **2013**, *10*, 20130512.

SUPPORTING INFORMATION

Additional supporting information may be found online in the Supporting Information section at the end of this article.

How to cite this article: Zhou Y, Alexandrov S, Nolan A, Das N, Dey R, Leahy M. Noninvasive detection of nanoscale structural changes in cornea associated with cross-linking treatment. *J. Biophotonics*. 2020;e201960234. <https://doi.org/10.1002/jbio.201960234>